2025 IEEE Applied Power Electronics Conference and Exposition (APEC) | 979-8-3315-1611-6/25/$31.00 ©2025 IEEE | DOI: 10.1109/APEC48143.2025.10977420

MagNetX: Foundation Neural Network Models for Simulating Power Magnetics in Transient

Shukai Wang[◇], Hyukjae Kwon[◇], Haoran Li[◇], Youssef Elasser[‡],
Gyeong-Gu Kang[◇], Daniel Zhou[◇], Davit Grigoryan[◇], and Minjie Chen[◇]
[◇]*Princeton University, Princeton, NJ, United States*
[‡]*Nvidia Research, Durham NC, United States*
Email: {sw0123, hk1715, minjie}@princeton.edu

***Abstract*—This paper introduces a foundation neural network framework for modeling power magnetics in transient, based on MagNetX[1] – a new extension of the MagNet database which includes extensive measurement data in transient. Provided with flux density $B(\mathrm{t})$ and field intensity $H(\mathrm{t})$ waveforms, the model uses partial memories and the next-state flux density excitation to predict the response of the field intensity in the next time step. The model is in time domain and is frequency independent. An example sequence-to-scalar LSTM neural network was designed, trained, and tested. This modeling framework can greatly enhance the modeling and design of power magnetics operating in transient condition, such as in PFCs and power amplifiers.**

***Index Terms*—power magnetics, hysteresis loop, machine learning, data-driven method, neural network, transformer.**

I. Introduction

Power magnetics are key components for storing energy in power electronic circuit designs, but they tend to be lossy and occupy a large volume, leading to less efficient and dense converter designs. Equation 1 depicts the relationship between volumetric core loss P_v and B-H loop. Material core losses exhibit highly nonlinear characteristics due to the intricate hysteresis mechanisms inherent in magnetic materials.

$$P_V = \frac{1}{T}\int_{B(0)}^{B(T)} H(t)\, dB(t) \tag{1}$$

The impact of frequency, temperature, dc-bias and other factors challenge existing loss and hysteresis models [1]. Most existing hysteresis models can be divided into two groups: traditional, or data driven method. Traditional magnetic hysteresis models include the Stoner-Wohlfarth model [2], the Jiles-Atherton model [3], and the Preisach model [4]. All three models can approximately trace the hysteresis curve but struggle to accurately capture magnetic behavior under specific operating conditions, especially temperature and dc-bias. While extended models and improved Steinmetz equations have been developed to address these limitations [5], most remain confined to static hysteresis analysis, and lacking the capability to model transient condition where the excitation behavior rapidly changes [6]–[9].

Most converter topologies, however, introduces transient conditions when the load behavior changes. In certain topology such as power factor correction boost converter–PFC Boost, contains composite inductor voltage and current waveform that is highly dynamic [10], [11]. Figure 1 depicts an example PFC boost inductor current as well as B-H loop waveform. Since the front-end provides a low frequency period ($2f_{Line}$), and back-end switches at much higher frequency (f_{Boost} = $100f_{Line}$), the inductor voltage and current are composite waveforms operating between two periods. Different from traditional static B-H loop, the slopes of the curve are dynamic in nature and the B-H position is heavily dependent on the past states. This highly complex hysteresis behavior renders the modeling of inductors in these topologies challenging.

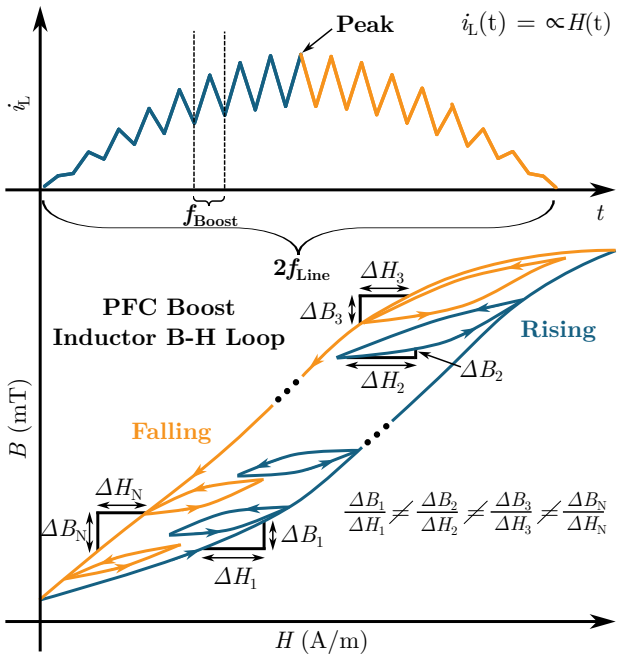

Fig. 1. Example of PFC-Boost multi-cycle transient B-H hysteresis: inductor current waveform and dynamic cycle transient condition with numerous minor loops.

The recent advanced data-driven method utilizing machine learning with neural network (NN) architectures have garnered much attention. Though there are techniques that predict hysteresis curves with simple neural network structures [12], or in combination with Preisach state memory [13], more advanced neural network structures such as LSTM [14] and Transformer

[1]MagNetX GitHub Repository: https://github.com/PaulShuk/MagNetX

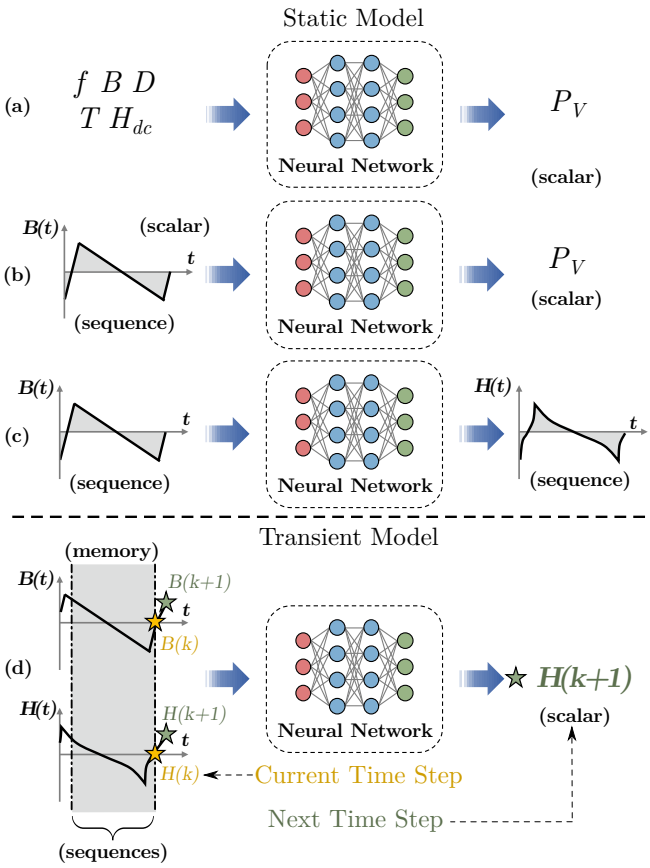

Fig. 2. A variaty of machine learning models: a) scalar-to-scalar; b) sequence-to-scalar; c) sequence-to-sequence; d) dual sequence-to-scalar models.

[15] based architecture have proven to be solving multi-variable non-linear regression problems with high accuracy [16]. Aiming to characterize core loss and hysteresis behaviors, MagNet[2] – an open-sourced core loss and static hysteresis database, built and deployed its first AI model for multiple soft ferrite materials utilizing both LSTM [17] and Transformer [18]. The MagNet project has created models for multiple purposes.

Figure 2a depicts a simple scaler-to-scaler neural network structure that maps scalar inputs of various operating parameters to volumetric core loss. However, this method is limited by its waveform types, hence not great for model generalization. As a result, time sequence $B(\mathrm{t})$ is introduced to the NN structure in Fig. 2b, which is capable of capturing arbitrary waveform type in its core loss model. The MagNet Challenge [19] yielded significantly more efficient and accurate neural network models for core loss modeling, advancing the Pareto frontier of modeling techniques. Lastly, the sequence-to-sequence model depicted in Fig. 2c is developed to map time sequence $B(\mathrm{t})$ to $H(\mathrm{t})$ for better exploration of a comprehensive steady-state hysteresis behavior [17], [18]. Figure 1a shows a seq-to-seq testing result of mapping a steady state full cycle B to its corresponding H sequence. The transformer model performed well at predicting correlations between two steady-state time sequences. All three models are trained based

[2]Princeton MagNet Project Website: https://mag-net.princeton.edu/

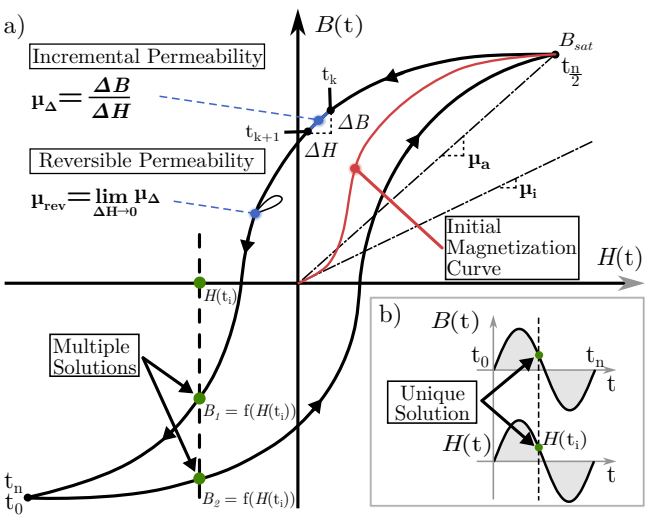

Fig. 3. Definitions of permeability on the B-H loop: a) static hysteresis loop on the B-H plane; b) B and H waveform on time-series scale.

on the steady-state full-cycle data provided in the MagNet database. In practice, however, power converters operate in both steady-state and transient conditions, rendering static models unable to correctly predict the transitional behavior between the steady-states. The existing models can not track a sequence with ever-changing duty cycles, or a full cycle with many minor loops as shown in Fig. 1b.

To model the transient behavior of power magnetics, a foundation neural network framework is needed which can generalize magnetic B-H behavior with minimal input constraints, eliminating the need to predefine specific parameters such as waveform type, frequency, or duty cycle. The key factor that governs the behavior of hysteresis curve is the precise relationship between $B(\mathrm{t})$ and $H(\mathrm{t})$ at any given time step. A pair of $B(\mathrm{t})$ and $H(\mathrm{t})$ sequences have a strong correlation and both exhibit memory effects. The excitation B in the subsequent state has a direct influence on the corresponding H, with their relationship additionally dependent on the system's previous state and the magnetic memory accumulated in recent states. Therefore, we extend the MagNet database to include transient data (the MagNetX database described in [20]), and propose a generalized MagNetX machine-learning framework for modeling the dynamic hysteresis behavior of materials. The new model is shown in Fig. 2d, predicting the future state based on the input of both B and H historical sequences.

The rest of the paper is organized as follows: Section II introduces the principles modeling B-H relations in dynamic state; Section III pictures the structure and the data flow of the LSTM-based Encoder-Projector architecture, modified from the existing MagNet sequence-to-sequence architecture; Section IV discusses how the training data is constructed; Section V shows the experimental results. Finally, Section VI concludes this paper.

II. Transient State Modeling

Ferromagnetic Material exhibits non-ideal hysteresis B-H loops shown in Fig. 3a. Permeability (μ) is the fundamental parameter governing magnetic hysteresis behavior, following

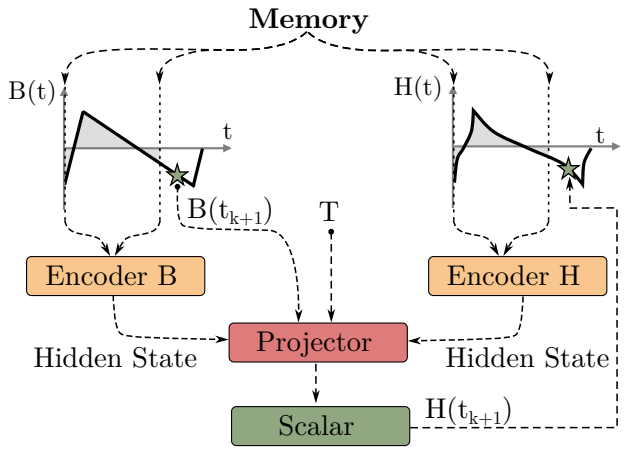

Fig. 4. Progression flow of the proposed neural network architecture. The system takes in both B and H memory sequences, and outputs the scalar H.

$B = \mu H$. However, numerous permeability types exist, with each defining distinct characteristics of the hysteresis curve, capturing different aspects of magnetic material behavior. Figure 3 presents the definition of various permeability types. Manufacturer often tends to provide either the initial permeability (μ_i), or amplitude permeability. Both are good metrics used for characterizing and classifying different materials, but lacks the ability to delineate the B-H loop on their own. On the hysteresis curve, the slope changes dynamically throughout the excitation cycle.

One could try generating a unique mapping between B and H to characterize dynamics for each hysteresis pair. Figure 3a has demonstrated, however, that if we apply an excitation of $H(t_i)$, a direct mapping could result in more than two non-identical solutions such as B_1 and B_2. To generate a unique mapping, we invoke the third dimension, time. As shown in Fig. 3b, time stamps can be used as tokens for each $B(t_k)$ - $H(t_k)$ pair which results in a unique solution. With each time sequence $B(\mathrm{t})$ and $H(\mathrm{t})$ bearing a total of n time steps, one may calculate a corresponding μ_Δ that yields a unique slope at each step. To calculate μ_Δ, or slope of the curve, information on the current time step $B(t_k)$, $B(t_k)$, $H(t_k)$, $B(t_{k+1})$, and $H(t_{k+1})$ needs to be known. The μ_Δ in this case is calculated as

$$\mu_\Delta = \frac{1}{\mu_0}\frac{\Delta B}{\Delta H} = \frac{1}{\mu_0}\frac{B(t_{k+1}) - B(t_k)}{H(t_{k+1}) - H(t_k)}, \tag{2}$$

where ΔB and ΔH are incremental changes of $B(\mathrm{t})$ and $H(\mathrm{t})$ from k^{th} time step to $(k+1)^{th}$ in a period. μ_Δ represents the slope of the B-H curve between the k^{th} and $(k+1)^{th}$ point. If the current time step excitation $B(t_k)$, $H(t_k)$ and μ_Δ are known, then given a new excitation $B(t_{k+1})$ in the next time step, the $H(t_{k+1})$ would be obtained by

$$H(t_{k+1}) = H(t_k) + \frac{B(t_{k+1}) - B(t_k)}{\mu_0 \mu_\Delta} \tag{3}$$

at any given time in a dynamic system. There are works that have attempted to utilize simple series interlinked feedforward neural networks to predict the μ_Δ [21], [22]. However, the model is restricted to the transient sequence that has a strong resemblance to sinusoids. The framework should be able to utilize the input information and correctly map out slope μ_Δ needed to obtain $H(t_{k+1})$. In the proposed setup, $H(t_{k+1})$ is directly used as the output of the system, since measurement data could introduce noises that result in a near-infinite μ_Δ slope between the current and next state. Thus, to better predict the corresponding response of the future state, the NN structure should at minimum include the information of the current time step B-H pair.

Algorithm 1 LSTM-based Sequence-to-Scalar Model

Input:
Segmented Flux Density $B_{mem}(t)$, Segmented Field Strength $H_{mem}(t)$, Next Step Flux Density $B(t_{k+1})$ Temperature T, Next Step Field Strength $H(t_{k+1})$ (only available in training);

Output:
Next Step Magnetic Field Strength $H(t_{k+1})$;

Initialize hideen states h_0 and cell states c_0;
$X_1 \leftarrow B(t_1)$;
$X_2 \leftarrow H(t_1)$;
for i = 1 to L **do**
  $h_i, c_i \leftarrow \mathrm{LSTM}_1\ (h_{i-1}, c_{i-1}, B(t_i))$ **[Encoder B]**
for i = 1 to N **do**
  $h_i, c_i \leftarrow \mathrm{LSTM}_1\ (h_{i-1}, c_{i-1}, H(t_i))$ **[Encoder H]**
$Y' \leftarrow \mathrm{FNN}(X_1,\ X_2,\ B(t_{k+1}),\ T)$; **[Projector]**
return $H(t_{k+1})$;

In addition, each state has strong dependencies on the waveform shape and trends of the immediate past. The presence of any distortion, ripple, large spikes, or noises may have different degrees of impact on the result of the next time step. Scalar inputs of the current state are not enough to represent the true behavior of the next time step. Therefore, the input of both B and H should both be sequences of most recent memories to properly describe the behavior of the next state. Thus the overall framework of the machine learning model revolves around utilizing a small portion of the immediate memory of both B-H pair for each time step to predict the immediate next state. The sequence-to-scalar framework is first used to predict all the $H(t_{k+1})$, then forming the whole sequence with all the scalar outputs as the fundamental building blocks.

III. Memory-Based LSTM Neural Network Structure

The LSTM is a commonly used NN framework that is best suited for sequential inputs solving complex regression problems [14]. Stock market predictions are good examples of applying LSTM networks to time series data with complicated dynamics [23]. The memory-based prediction of arbitrary waveforms is conceptually similar to the prediction of stock prices, both involving complex, nonlinear time-series prediction challenges that require capturing historical patterns and state-dependent dynamics. Therefore, as shown in Fig. 4, we select memory sequence $B(\mathrm{t})$ and $H(\mathrm{t})$ as input sequences. The output is the next state field intensity $H(t_{k+1})$. From Eq. 2, the future step $B(t_{k+1})$ is necessary for informing the $H(t_{k+1})$. In addition, variable such as temperature externally

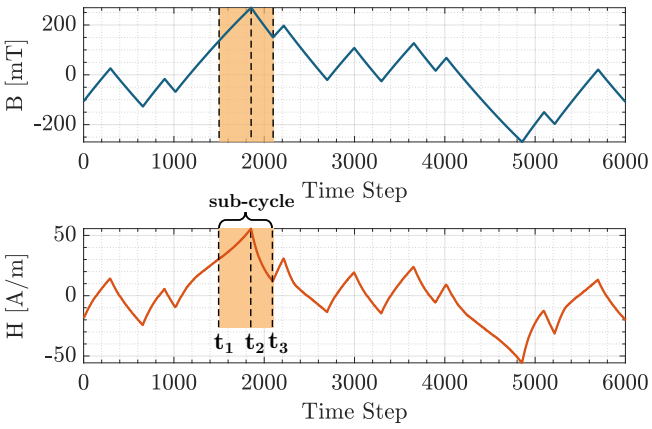

Fig. 5. Example measurement $B(t)$ and $H(t)$ data sequence. Waveform contains 10 cycles of data that is sampled with 6,000 points.

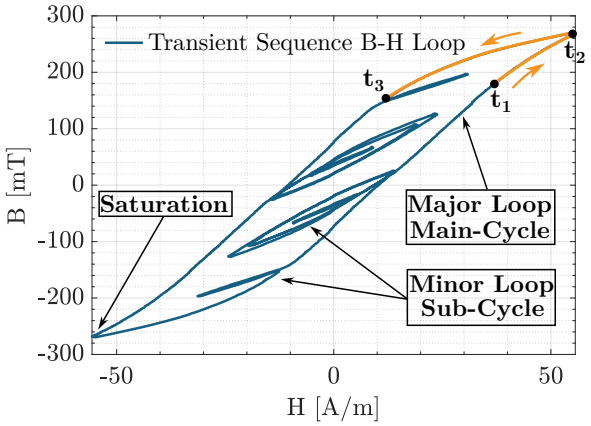

Fig. 6. A single B-H loop, with many transient minor loops, echoing the behavior found in Fig 5.

influences the hysteresis behavior as well. Therefore, a projector module is placed past the encoder stage, where the scalar input of the $B(t_{k+1})$, and temperature (T) are implemented. Other variables such as frequency, dc-bias, and duty cycle are not necessary as explicit inputs since the time series data $B(\mathrm{t})$ and $H(\mathrm{t})$ intrinsically encode their information.

In the proposed NN structure, memory segments $B(\mathrm{t})$ and $H(\mathrm{t})$ are individually fed through separate LSTM modules to address the temporal correlation of the most recent memories to the distant past. LSTM module will first characterize the individual sequence by memorizing only the important information such as the waveform's turning points, peaks, and troughs. Then, the output of the LSTM cells provides the updates of the hidden states and is loaded into the feedforward neural network (FNN). With the provided $B(t_{k+1})$ and T as scalar inputs to the FNN, the projector performs the learning process to determine the output $H(t_{k+1})$. The detailed architecture can be described in Fig. 7. The training flow of the model are detailed in the pseudo code in Algorithm 1.

IV. Data Collection and Processing

High quality machine learning model always rely on high quality database. MagNet database collects data using the four wire method [24], and controls frequency under 500 kHz to minimize probe delay error. A T-type inverter is used as the power stage to provide excitations to the windings of the core under test (CUT). The previously open-sourced data only contain steady-state voltage $v(t)$ and current $i(t)$ pairs. In order to model the transient hysteresis, MagNet database is updated with new triangular current dynamic data for 10 materials [20]. The corresponding data collection sequence is developed aiming at providing transient data measurement. The transient data is created by creating sequences of randomly changing duty cycles during each period of switching. The voltage current sequences are inferred to corresponding B-H pairs.

Figure 5 shows an example data collection of B and H waveforms under triangular (current) excitation. Step changes are applied by varying random sequence of duty cycle changes. The CUT is excited with 10 transient sub-cycles forming the main cycle. The sub-cycles are excited at 50 kHz, whereas the total excitation period is 5 kHz. Each sub-cycle is represented as the minor loops on the B-H curve in Fig. 6. The sub-cycles together form a major cycle, mimicking transient hysteresis conditions. As current increases, the CUT undergo saturation which can be observed in the H waveform as well as the B-H loop. The exampled waveform is post processed by down sampling to 600 points per sub-cycle.

There are various number of combinations when applying the voltage duty cycle step changes. Magnetics react differently when voltage excitation changes from 20% to 50% verses from 80% to 50%. Same set of duty cycles step changes at 50 kHz and 500 kHz also appear to be different. The model is likely to benefit from a highly diverse and extensive combinations of step changes. In the final database, each sequential data contains 100 normalized distributed random duty cycle step changes to enrich the diversity of magnetic response to various transient states. A total of 13,587 sequences of data is collected for 3C90, including frequencies ranging from 50 kHz to 800 kHz at three temperatures (25, 50, 70 °C). Given the horizontal resolution of the oscilloscope, 100 sub-cycle sequence achieves a good balance between waveform degradation and combination richness. Figure 8 showcases one of such sequence. Each long sequence is downsampled to 2,000 points for the whole period, or 20 points per sub-cycle. This is the maximum amount of downsampling before the loss of critical information. In addition, the data is prone to having noises and sharp spike due to circuit network's capacitive effect during testing. Therefore, a post-processed software filter was also applied to eliminate data with extremely large slopes to avoid confusion with true step changes in training.

Figure 8 showcases an example downsampled data sequence being prepared for training. In this example, The CUT employs material Ferroxcube 3C90. The original sequence length is sampled with 2000 points which is represented by $B(t_{k+1})$ and $H(t_{k+1})$ respectively. For training such a sequence, the model takes each $H(t_{k+1})$ point as an output. This implies that each $H(t_{k+1})$ is associated with a corresponding $B(t_{k+1})$ scalar input and both B_{mem} and H_{mem} segmented memory as sequence inputs. The model's input encompasses both the current excitation point $B(t_k)$ and $H(t_k)$ and several preceding states near the present time step, with the number of past states determined by the strength of the material's memory effect. Since a single 100 sub-cycle period is continuous from

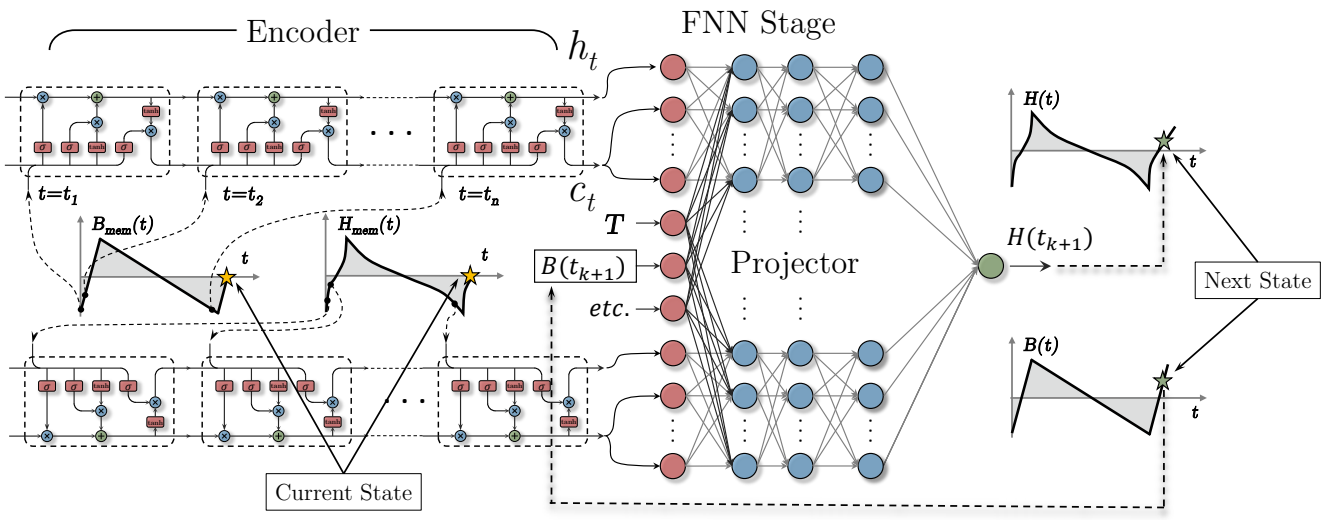

Fig. 7. Overview of the dual encoder, projector architecture. The model takes in two segmented memory inputs and each point on the sequence is fed sequentially into concatenated LSTM cell. The projector then takes in the hidden, and cell states into the projector. The next state $B(t_{k+1})$ and $H(t_{k+1})$ are siphoned from the original sequence and fed into the projector and output.

the end to the beginning, a segment length equivalent to the memory window size is copied and appended in front of the sequence for the training of the first few points. The specific segmented memory points chosen for material 3C90 is selected as 60. When selecting window range, there are a couple important considerations.

(1) **Memory Length:** Theoretically, the magnetic remanence lasts indefinitely, making every historical point relevant to future excitation behavior. However, given the data storage limit, it is acceptable to "remember" only the most recent few cycles depending on the gravity of the memory effect tailored to each specific material.

(2) **Peak Values:** The local peaks and troughs are of high significance in determining future excitation states, exerting greater influence than other historical points in the sequence. It may be crucial to selectively store the positive and negative peaks values from distant past sub-cycles, rather than the entire waveform data.

The memory is selected based on the memory effect of the highest frequency (500 kHz as tested) as it sees more dynamic changes in the past number of points than any other frequencies. Given that 60 points are chosen for each segmented memory sequences, the selected material only retains memory of the past 3 cycles. As seen in Fig 8, each sub-cycle in the memory window inherit a different duty cycle excitation.

V. Neural Network Training and Testing

For training the neural network, 600 sequences comprised of frequencies from 50 kHz, 200 kHz, and 500 kHz at 25°C are selected. Since each sequence contains 2000 output points for training, the total sets of output data is 1,200,000, with 2,400,000 input sequences. The final post processed data size is 2.0 GB. The LSTM-based encoder-projector sequence-to-scalar model is synthesized with the PyTorch framework. Hyper-parameters of the network structure are determined and optimized based on experimental training results. For the model proposed in this work, both LSTM cells have 32 cell states and 32 hidden states. The output of the LSTM cells are fed into the projector which comprises 3 layers with 64 neurons in the first two layers, and 32 neurons in the third layer. The total number of parameters trained for the model is 19,587. The mean-squared error (MSE) between the predicted scalar output $H_{pred}(t_{k+1})$ and the measured $H_{meas}(t_{k+1})$ is selected as the loss function for the backpropagation during training. The proposed framework was trained with 3,000 epochs using the Princeton Research Computing Della Cluster on the Nvidia A100 80GB GPU devices. The total training took around 4 hours.

There are two steps to evaluating the model. Step 1: The model is to be tested with the measured dataset of H_{mem}, to validate the robustness of the model at predicting the next time step point. Step 2: The H_{mem} is updated iteratively, incorporating the newly predicted value from the previous iteration. If the first step demonstrates highly accurate prediction, only then will the second step be considered. The trained LSTM model in this paper is evaluated on the test set based on the implementation of the first step. The testing dataset employs the 600 sequences at 25 °C. All data are tested and recorded as scalar outputs, before all 2,000 points are synthesized to form the sequence again. Figure 9 depicts the model prediction of the dataset compared to the raw dataset. The model makes prediction closely matches with the measurement result, even during the saturation period. A zoomed in view provides a more detailed look at the prediction accuracy. The figure on the very right represents the final converged results. As the training proceeds, the model gradually converges and the discrepancy between the predicted and the measured hysteresis loops is minimized, eventually achieving a good match.

In addition, a reference $H(\mathrm{t})$ is calculated using Eq. 2 by replacing μ_Δ with initial permeability μ_i, which is depicted in the Fig. 9. The μ_i used for material 3C90 is 2300. As observed, at very low excitation levels, the incremental permeability,

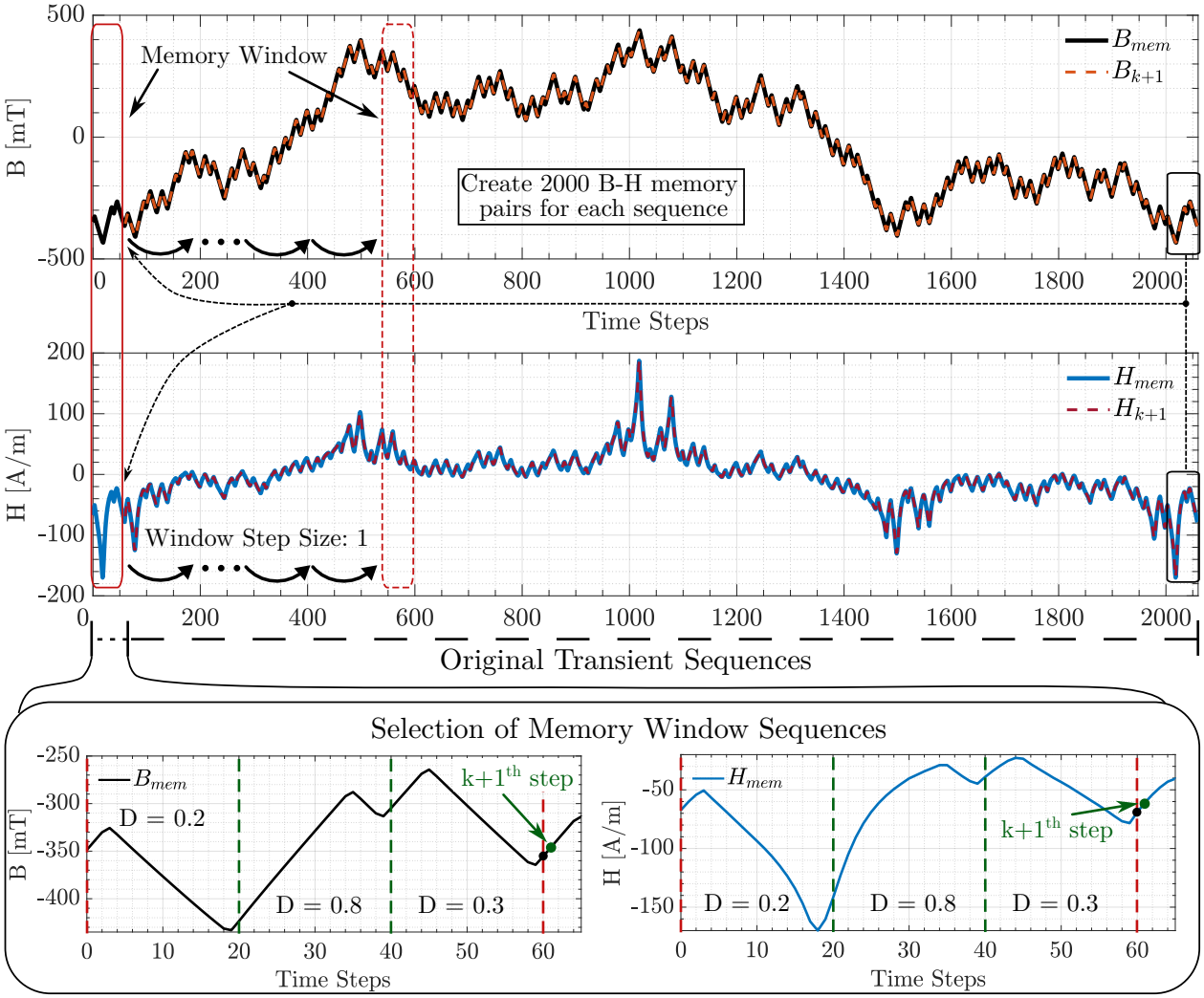

Fig. 8. Updated MagNet database (the MagNetX database) including transient sequences. Each large cycle contains 100 step change duty cycles. The last window size is copied and appended to the beginning. Each window is sized with 60 point memories.

μ_Δ is much larger than 2300, hence the calculation with μ_i induces a larger slope of in the H sequence, deviating from true measurements. On the contrary, when the core reaches saturation, μ_i becomes greater than μ_Δ, resulting in the calculated H sequence being unable to reach the magnitude it would otherwise in a true saturation condition.

Even though the model predicts scalar outputs, the accuracy of the model is still quantified by calculating the relative error between the predicted sequence $H_{pred}(t)$ and the measured sequence $H_{meas}(t)$ of the entire cycle at once. The relative error of the sequence is calculated as:

$$\text{Relative Err. of Sequence} = \frac{\text{rms}(H_{pred} - H_{meas})}{\text{rms}(H_{meas})} = \frac{\sqrt{\frac{1}{n}\sum_{t=t_1}^{t_n}\left(H_{pred}(t) - H_{meas}(t)\right)^2}}{\sqrt{\frac{1}{n}\sum_{t=t_1}^{t_n}\left(H_{meas}(t)\right)^2}} \quad (4)$$

Figure 10 demonstrates the distribution of relative errors in the predicted $H(\mathrm{t})$ sequences in the test set generated by the transformer-based model. As shown in the figure, the model is capable of accurately predicting the $H(\mathrm{t})$ sequence with an average, and 95th percentile of the sequence relative error of 3.81% and 6.552% respectively. These statistics on the prediction results provided good evidence that the proposed model is capable of making accurate predictions for the hysteresis loops under various operating conditions.

In order to validate the model's capabilities of handling various frequency, another test dataset is created. Compared to the training data which contains 600 sequences operating at frequencies 50 kHz, 200 kHz, and 500 kHz, the test data contains 600 data sequences of 80 kHz, 125 kHz, and 320 kHz. The test dataset introduces 100% of new data. Figure 12 presents one of such prediction, measurement sequence at 200 kHz. The predicted result still managed to achieve reasonable results, with predictions having slight deviations from the measurement data. Another characteristic of the model is that the prediction always has slight delay at sharp transitions where the slope of H changes from positive to negative. Such delay could be minimized by increasing the resolution of the

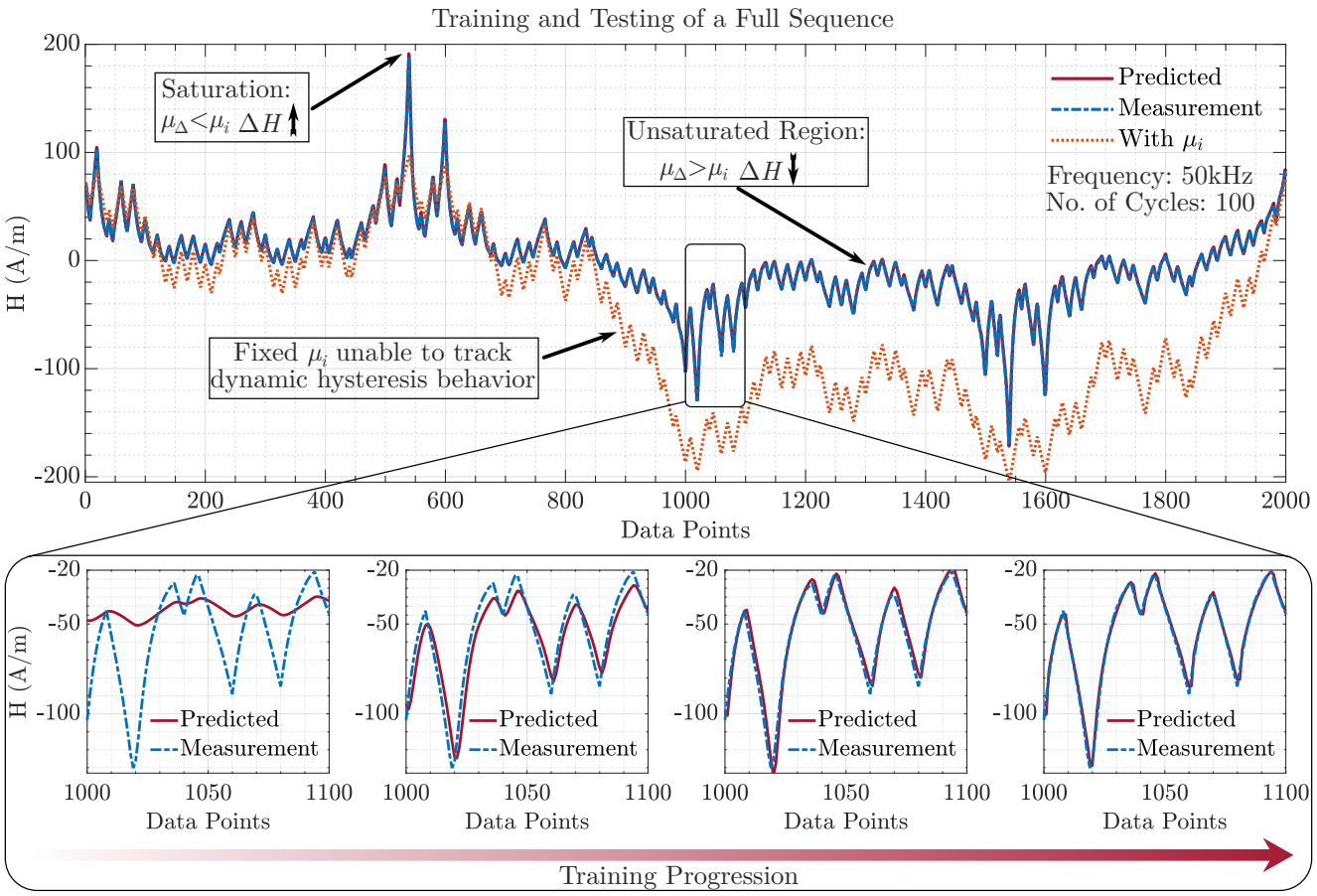

Fig. 9. The testing of the full sequence. Sequence includes low flux excitations as well as saturation point. A comparison of predicted and calculated waveform using initial permeability μ_i. The neural network model shows much better prediction results compared to a fixed permeability approximation.

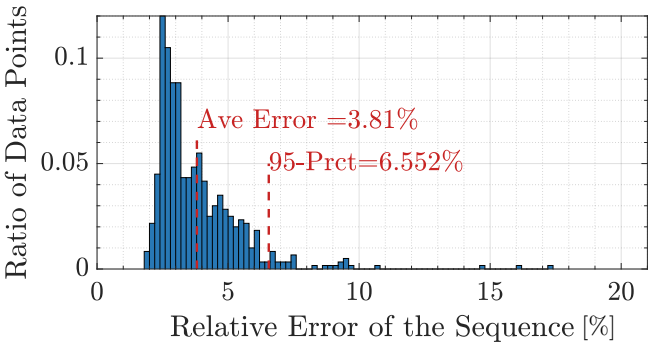

Fig. 10. Relative error of the sequence between predicted and measured result. The average error is calculated based on the result of the testing data and training data of the same frequency.

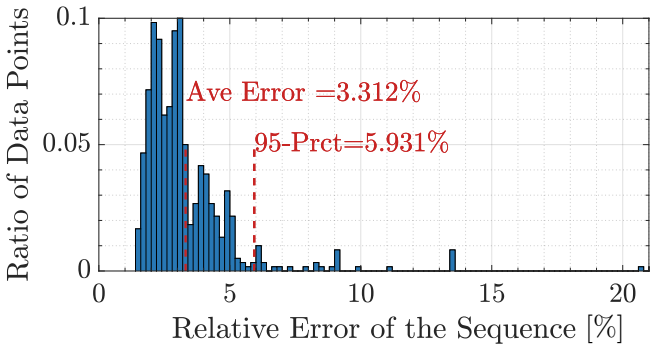

Fig. 11. Relative error of the sequence comparing the training dataset and new test dataset on frequencies that the original training dataset does not cover.

sequence. The average error and 95%th error are 3.312% and 5.931% respectively. The comparison indicates that the performance of the model with data of different frequency is comparable to the data tested with the original training data. The model demonstrates reasonable generalization capability.

VI. Conclusions

This paper introduces a foundation neural network framework for modeling magnetic hysteresis under transient excitations, and presents an LSTM-based encoder-projector sequence-to-scalar neural network architecture. The developed model takes its first step towards a foundational model that is capable of modeling complex hysteresis behaviors in transient. An example LSTM neural network model was designed, trained, and tested, validating the effectiveness of the proposed architecture. This breakthrough sparked a new approach to modeling complex magnetic behaviors, aiming to accurately predict B–H relationships by incorporating both material characteristics and memory effects, moving beyond the limitations of fixed frequency periodic steady state assumptions.

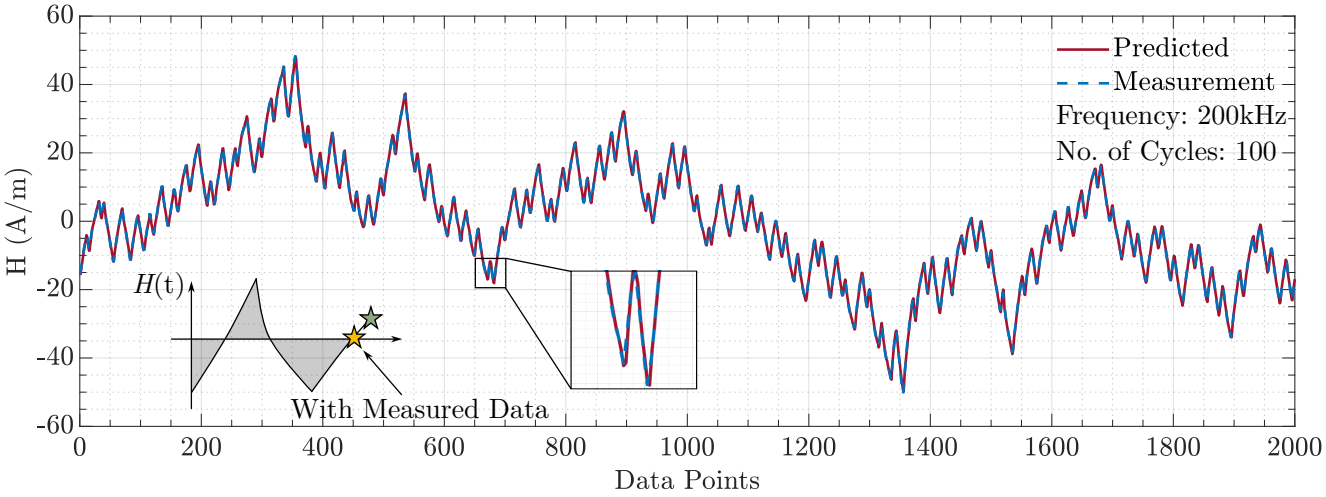

Fig. 12. Test dataset with different frequency values as the training dataset. The neural network model was able to accurately predict the material response even though the training data and testing data were collected at different frequencies.

ACKNOWLEDGEMENTS

This work was jointly supported by the National Science Foundation under Award #2344664, ITG Electronics, TSMC, pSemi, and the Princeton Andlinger Center for Energy and the Environment.

REFERENCES

[1] D. Serrano, H. Li, S. Wang, T. Guillod, M. Luo, V. Bansal, N. K. Jha, Y. Chen, C. R. Sullivan, and M. Chen, "Why magnet: Quantifying the complexity of modeling power magnetic material characteristics," *IEEE Transactions on Power Electronics*, vol. 38, no. 11, pp. 14 292–14 316, 2023.

[2] E. C. Stoner and E. P. Wohlfarth, "A mechanism of magnetic hysteresis in heterogeneous alloys," *Philosophical Transactions of the Royal Society of London. Series A, Mathematical and Physical Sciences*, vol. 240, no. 826, pp. 599–642, 1948. [Online]. Available: https://royalsocietypublishing.org/doi/abs/10.1098/rsta.1948.0007

[3] D. Jiles and D. Atherton, "Theory of ferromagnetic hysteresis," *Journal of Magnetism and Magnetic Materials*, vol. 61, no. 1, pp. 48–60, 1986. [Online]. Available: https://www.sciencedirect.com/science/article/pii/0304885386900661

[4] F. Preisach, "Über die magnetische Nachwirkung," *Zeitschrift fur Physik*, vol. 94, no. 5-6, pp. 277–302, May 1935.

[5] H. H. Cui, S. Dulal, S. B. Sohid, G. Gu, and L. M. Tolbert, "Unveiling the microworld inside magnetic materials via circuit models," *IEEE Power Electronics Magazine*, vol. 10, no. 3, pp. 14–22, 2023.

[6] A. Raghunathan, Y. Melikhov, J. E. Snyder, and D. C. Jiles, "Modeling the temperature dependence of hysteresis based on jiles–atherton theory," *IEEE Transactions on Magnetics*, vol. 45, no. 10, pp. 3954–3957, 2009.

[7] R. Szewczyk, A. Bieńkowski, and J. Salach, "Extended jiles–atherton model for modelling the magnetic characteristics of isotropic materials," *Journal of Magnetism and Magnetic Materials*, vol. 320, no. 20, pp. e1049–e1052, 2008, proceedings of the 18th International Symposium on Soft Magnetic Materials. [Online]. Available: https://www.sciencedirect.com/science/article/pii/S0304885308005556

[8] H. Cui and K. D. T. Ngo, "Transient core-loss simulation for ferrites with nonuniform field in spice," *IEEE Transactions on Power Electronics*, vol. 34, no. 1, pp. 659–667, 2019.

[9] M. Chen, S. Chakraborty, and D. J. Perreault, "Multitrack power factor correction architecture," *IEEE Transactions on Power Electronics*, vol. 34, no. 3, pp. 2454–2466, 2019.

[10] J. P. M. Figueiredo, F. L. Tofoli, and B. L. A. Silva, "A review of single-phase pfc topologies based on the boost converter," in *IEEE/IAS International Conference on Industry Applications*, 2010, pp. 1–6.

[11] T. Jappe, M. Lohn, and S. Mussa, "Gan-based single-phase bridgeless pfc boost rectifier," *The Journal of Engineering*, vol. 2019, 04 2019.

[12] Z. Zhao, F. Liu, S. L. Ho, W. N. Fu, and W. Yan, "Modeling magnetic hysteresis under dc-biased magnetization using the neural network," *IEEE Transactions on Magnetics*, vol. 45, no. 10, pp. 3958–3961, 2009.

[13] C. Serpico and C. Visone, "Magnetic hysteresis modeling via feed-forward neural networks," *IEEE Transactions on Magnetics*, vol. 34, no. 3, pp. 623–628, 1998.

[14] S. Hochreiter and J. Schmidhuber, "Long short-term memory," *Neural Comput.*, vol. 9, no. 8, p. 1735–1780, Nov. 1997. [Online]. Available: https://doi.org/10.1162/neco.1997.9.8.1735

[15] A. Vaswani, N. Shazeer, N. Parmar, J. Uszkoreit, L. Jones, A. N. Gomez, Ł. Kaiser, and I. Polosukhin, "Attention is all you need," in *Advances in neural information processing systems*, 2017, pp. 5998–6008. [Online]. Available: http://arxiv.org/abs/1706.03762

[16] Y. LeCun, Y. Bengio, and G. Hinton, "Deep learning," *Nature*, vol. 521, pp. 436–44, 05 2015.

[17] H. Li, D. Serrano, S. Wang, and M. Chen, "Magnet-ai: Neural network as datasheet for magnetics modeling and material recommendation," *IEEE Transactions on Power Electronics*, vol. 38, no. 12, pp. 15 854–15 869, 2023.

[18] H. Li, D. Serrano, T. Guillod, S. Wang, E. Dogariu, A. Nadler, M. Luo, V. Bansal, N. K. Jha, Y. Chen, C. R. Sullivan, and M. Chen, "How magnet: Machine learning framework for modeling power magnetic material characteristics," *IEEE Transactions on Power Electronics*, vol. 38, no. 12, pp. 15 829–15 853, 2023.

[19] M. Chen *et al.*, "Magnet challenge for data-driven power magnetics modeling," *IEEE Open Journal of Power Electronics*, pp. 1–16, 2024.

[20] H. Kwon, S. Wang, H. Li, Y. Elasser, G.-G. Kang, D. Zhou, D. Grigoryan, and M. Chen, "Magnetx: Extending the magnet database for modeling power magnetics in transient," in *2025 IEEE Applied Power Electronics Conference and Exposition*, 2025.

[21] A. Laudani, G. M. Lozito, and F. Riganti-Fulginei, "Dynamic hysteresis modelling of magnetic materials by using a neural network approach," *2014 AEIT Annual Conference - From Research to Industry: The Need for a More Effective Technology Transfer, AEIT 2014*, 01 2015.

[22] A. Laudani, G. M. Lozito, F. R. Fulginei, and A. Salvini, "Modeling dynamic hysteresis through fully connected cascade neural networks," in *International Forum on Research and Technologies for Society and Industry Leveraging a better tomorrow (RTSI)*, 2016, pp. 1–5.

[23] A. Moghar and M. Hamiche, "Stock market prediction using lstm recurrent neural network," *Procedia Computer Science*, vol. 170, pp. 1168–1173, 2020, the 11th International Conference on Ambient Systems, Networks and Technologies (ANT) / The 3rd International Conference on Emerging Data and Industry 4.0 (EDI40) / Affiliated Workshops. [Online]. Available: https://www.sciencedirect.com/science/article/pii/S1877050920304865

[24] S. Wang, H. Li, D. Serrano, T. Guillod, J. Li, C. Sullivan, and M. Chen, "A simplified dc-bias injection method for characterizing power magnetics using a voltage mirror transformer," *IEEE Transactions on Power Electronics*, vol. 39, no. 6, pp. 6608–6612, 2024.